

Carrier Dynamics and Morphology Regulated by 1,8-Diiodooctane in Chlorinated Nonfullerene Polymer Solar Cells

Hui Chen,^{†,||} Jianfei Qu,^{†,||} Longzhu Liu,[†] Wei Chen,^{‡,§} Feng He^{*,†}

[†]Department of Chemistry and Shenzhen Grubbs Institute, Southern University of Science and Technology, Shenzhen 518055, China.

[‡] Materials Science Division, Argonne National Laboratory, 9700 Cass Avenue, Lemont, Illinois, 60439, United States.

[§] Institute for Molecular Engineering, The University of Chicago, 5640 South Ellis Avenue, Chicago, Illinois, 60637, United States.

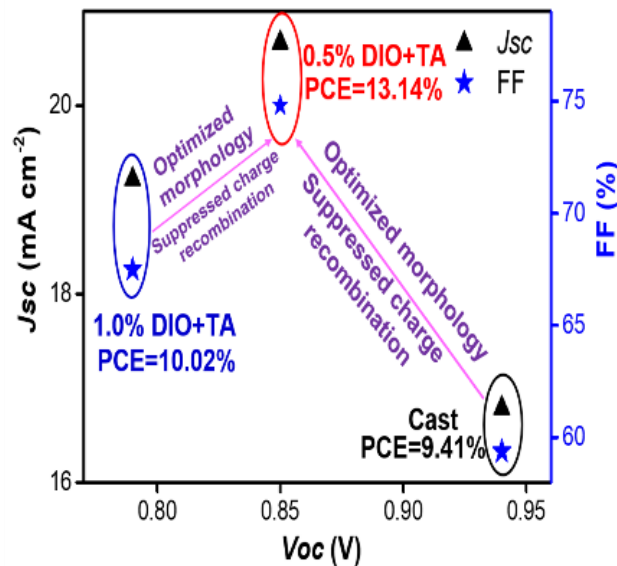
Corresponding Author

E-mail: hef@sustc.edu.cn

ABSTRACT:

Very small amounts of 1,8-diiodooctane (DIO) are very effective to optimize the performance of polymer solar cells (PSCs). So far, the underlying influences are not yet fully understood, especially in non-fullerene PSCs. Herein, the influence of DIO on carrier dynamics and morphology in PBDBT2Cl:IT4F system were investigated in detail. We combined the characterization of the transient dynamics with the morphology characterization of PSC devices to explore the origin of enhanced performance. Compared to the cast device, the champion device with 0.5% DIO revealed the maximum of current density (J_{sc}) and fill factor (FF). The optimum DIO content helps to enhance carrier transport and optimize morphology while excess of DIO produces adverse effects due to the induced intense aggregation and dilated size in blend films. The results provide some hints of improved device performance upon the DIO as an additive in non-fullerene PSCs.

TOC Graphic



Bulk-heterojunction (BHJ) polymer solar cells (PSCs) based on a blend of conjugated polymer donor and fullerene or non-fullerene derivatives have attracted enormous attention within the last decade.¹⁻⁵ PSCs possess some unique advantages such as low-cost, light-weight, and solution-processed large-scale fabrication.⁶⁻⁹ The abundant and excellent advances in material synthesis and interface engineering of PSCs have emerged, leading to the power conversion efficiencies (PCEs) of single-junction PSCs above 14%.¹⁰⁻¹⁵ Especially in the material design path-breaking chlorination atomic substitution was extensively studied on both donors and non-fullerene acceptors. The more progress in chlorinated PSCs has been achieved, the chlorinated polymer exhibited the better photovoltaic performance than the fluorinated polymer in some special cases.¹⁵⁻¹⁸ Among the halogens, fluorine is the most electrophilic and smallest in atom size. However, chlorine has a larger atom radius and is the second most electrophilic candidate among the halogens. Analogously, chlorination reveals the similar effects as fluorine in polymers and the corresponding solar cells and meanwhile the synthesis of the chlorine-containing polymers is facile.¹⁷ Besides, empty 3d orbitals of chlorine can accommodate lone pair electrons while fluorine does not have energetically accessible empty orbitals for such delocalization. At last, the synthesis of the chlorinated polymers showed to be easier with higher yield than fluorination and finally lower cost of raw materials for roll-to-roll printing products.¹⁶

Apart from the high-quality material synthesis, optimization of device processing is also very important to performance of PSCs.¹⁹ Numerous approaches were successfully applied into optimization of device processing, and morphology control of the active layer played a critical role in device performance. The popular and universal measurements, such as use of additives,¹⁹ thermal annealing,²⁰ and solvent vapor annealing,²¹ have been widely used in neat film

preparation. Among these methods, the use of solvent additives has demonstrated to be particularly effective and convenient in PSCs. The proper independent and blend domain sizes of polymer donor and small molecule acceptor could be controlled by their different solubility to solvent additives.¹⁹ The most frequently-used solvent additive is 1,8-diiodooctane (DIO) with higher boiling point compared to conventional processing solvent. Thus, the extended time of volatilization promotes the organized domain formation in the blend. For instance, PTB7:PC₇₁BM devices with DIO treatment presented the very high performance compared to the as-cast device. A similar behavior was also found in other efficient polymers.¹⁹

Recently, plentiful non-fullerene (NF) acceptors with excellent photovoltaic properties have been designed and synthesized.^{1,6} Currently, the PCE of non-fullerene PSCs goes beyond 14% exceeding the highest level of the fullerene counterparts.¹⁰⁻¹⁵ Although fullerene and non-fullerene materials exhibit many differences in morphology and charge separation mechanism, the addition of DIO is still important to device processing solvent for efficient NF-PSCs, except that the amount of DIO was reduced in isopycnic solvent. The optimum morphology of NF-PSCs should exhibit efficient exciton separation and charge transport within the device, however, this is difficult to predict and to control. The active layer morphology is formed by polymer donor, small molecular acceptor and mixed donor-acceptor (D-A) domains²². DIO as additive can control the domains sizes, size distribution and domain purity, which are all crucial to performance of NF-PSCs. Although the DIO amount is very small, it is effective to optimize the blend morphology facilitating enhanced charge transport in active layer of device.^{12,15}

A previous study reported that the use of DIO in the processing solvent of PBDBT2Cl:IT4F yielding very high PCE, which is extremely supportive for the use of chlorinated polymers.¹⁵ The previous research was mainly focusing on the design and synthesis of polymer. In this contribution, we systematically investigated the effect of DIO content on the carrier dynamics and blend morphology in this system. For champion devices, the short-circuit current (J_{sc}) and fill factor (FF) are obviously enhanced, but the V_{oc} is remarkably lower

compared to as-cast devices. To better understand the origin of enhanced device performance, we combined the morphology investigations with transient dynamics studies.

Table 1. The performance parameters of PSCs with various DIO content in solvent under 100 mW cm⁻² AM 1.5 G irradiation.

Treatments	V_{oc} [V]	J_{sc} [mA cm ⁻²]	FF [%]	PCE [%]
A: As-cast	0.94	16.79	59.38	9.41
B: 0.5% DIO+TA	0.85	20.67	74.81	13.14
C: 1.0% DIO+TA	0.79	19.22	67.49	10.02

The chemical structures of polymer PBDBT2Cl and IT4F are shown in Figure 1a. Both substances were synthesized in our laboratory according to previous reports.^{15,23} We used an inverted device structure of ITO/ZnO/PBDBT2Cl:IT4F/MoO₃/Ag to study the device performance of PSCs with different amount of DIO in the chlorobenzene solvent. The detailed relationship between device performance with the DIO contents is summarized in Table S1 and Figure S1. With gradually increasing DIO percent content in the solvent, the V_{oc} of corresponding devices steadily declines (see Figure S2). However, J_{sc} and FF increase first and then decrease with a maximum at about 0.5% DIO content. To improve the device performance, we used thermal annealing to all devices. The treatment resulted in a small decline of V_{oc} while J_{sc} and FF increased in value.

For further discussion, we select three representative devices. Device A is the as-cast device without any treatment. Devices B and C are prepared with 0.5% and 1% DIO as additive, respectively, and then thermal annealing of both blend films at 100°C for 10 minutes. Table 1 summarizes the performance of the investigated devices. The corresponding current density-voltage (J - V) curves are shown in Figure 1b. Device A has a moderate PCE of 9.41% with J_{sc} of 16.79 mA cm⁻² and FF of 59.38%, but the V_{oc} is rather high (0.94 V). Device B yielded a significantly higher PCE of 13.14%, attributed to the drastically enhanced J_{sc} of 20.67 mA cm⁻² and FF of 74.81%. Compared to device A, the V_{oc} of device B had negligible reduction (V_{oc}

= 0.85 V). With further increase of DIO content (device C), the V_{oc} reduces to 0.79 V. The other parameters were also found to be lower than device B. From the external quantum efficiency (EQE) spectra in Figure 1c, device A showed the response peak at 570 nm in the main absorption region of PBDBT2Cl, the response peak of device C was at 730 nm in the main absorption region of IT4F. The normalized UV-Vis absorption spectra of PBDBT2Cl and IT4F are shown in Figure 1d. After the device processing with DIO, the EQE responses of near the IT4F absorption region were largely increased, highlighting the light current contribution from IT4F, which was also observed from the normalized EQE in Figure 1e.

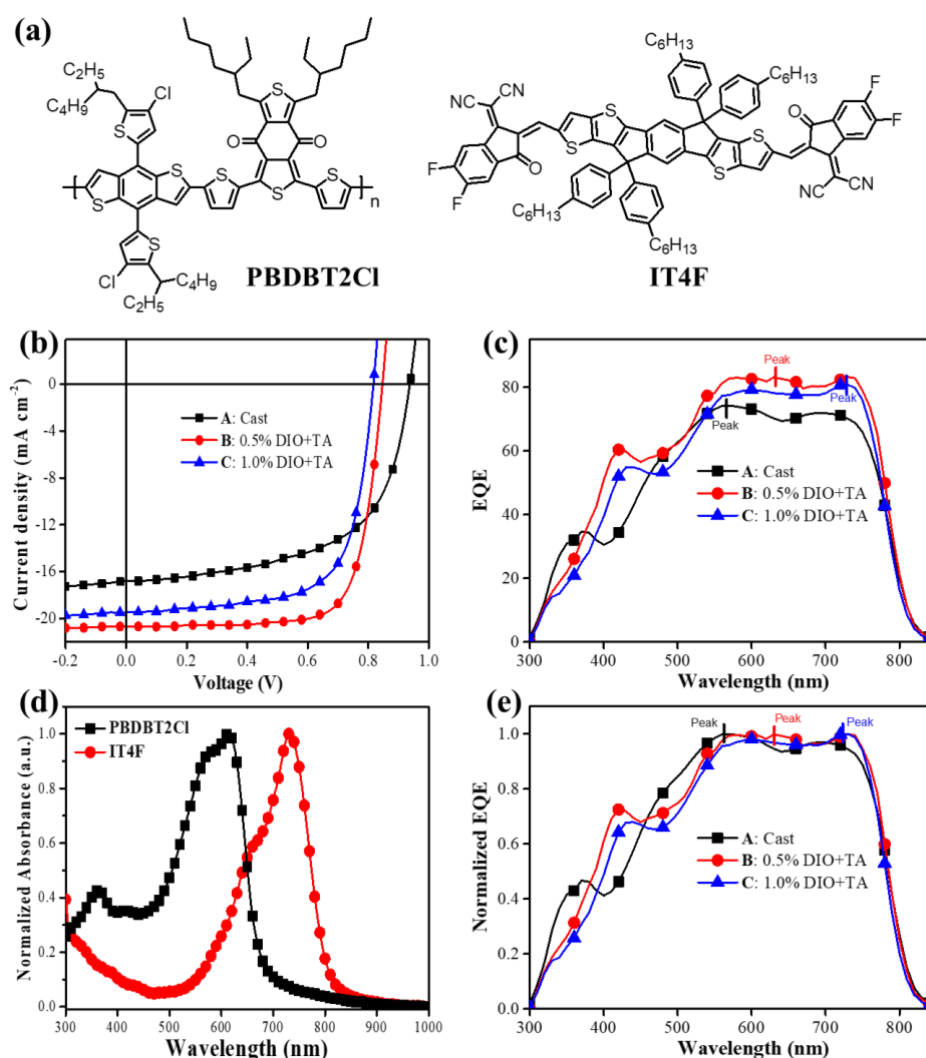


Figure 1. (a) Chemical structures of PBDBT2Cl and IT4F; (b) J - V and (c) EQE curves of PSCs with various DIO content; (d) the absorption of PBDBT2Cl and IT4F films; (e) Normalized EQE curves of PSCs with various DIO content.

The reduction of V_{oc} and enhancement of J_{sc} and FF are very closely related to carrier mobility for the devices with DIO processing. We used the space-charge-limited current (SCLC) method²⁴ and fabricated the single carrier devices to determine the mobility of hole and electron for corresponding solar device. The J - V characteristics of single carrier devices are shown in the Figure 2, the fitted and extracted values of mobility were listed in Table S2. The hole and electron mobility of as-cast device were in a lower range with values of $9.6 \times 10^{-5} \text{ cm}^2 \text{ V}^{-1} \text{ S}^{-1}$ and $6.8 \times 10^{-5} \text{ cm}^2 \text{ V}^{-1} \text{ S}^{-1}$, respectively. Such moderate mobility may cause charge accumulation in the active layer, which is a restrictive factor leading to the poor J_{sc} and FF. In contrast device B with 0.5% DIO content showed hole mobility was up to $3.4 \times 10^{-4} \text{ cm}^2 \text{ V}^{-1} \text{ S}^{-1}$, and the electron mobility also improved to $2.6 \times 10^{-4} \text{ cm}^2 \text{ V}^{-1} \text{ S}^{-1}$. As a result of the enhanced and balanced mobility of carriers, the whole device performance sharply increased due to significant enhancement of J_{sc} and FF. However, the V_{oc} decreased to 0.85 V, which can be attributed to shorten the quasi-Fermi levels between electrons and holes upon increased charge carrier mobility.²⁵ For DIO contents of about 1%, the hole and electron mobility both descended, resulting in simultaneous reduction in every parameter to the best device. Unexpectedly, the V_{oc} further decreased to 0.79 V. Unlike the previous tendency, the sacrificial V_{oc} cannot bring about the improvement of mobility and J_{sc} . To get further insight the response of J_{sc} versus varying light intensities (I) was tested and used to probe the charge recombination in steady state (see Fig. S3). The relationship of J_{sc} and I is formulated by $J_{sc} \propto I^\alpha$.²⁶ The α values deduced from Figure S3 of device A, B and C are 0.90, 0.99 and 0.94, respectively. As expected, the device B with best performance exhibited highest value. The reduced value for device C indicates that the bimolecular recombination was more extensive compared to the device B. This is also a possible factor for the origin of reduced device performance.

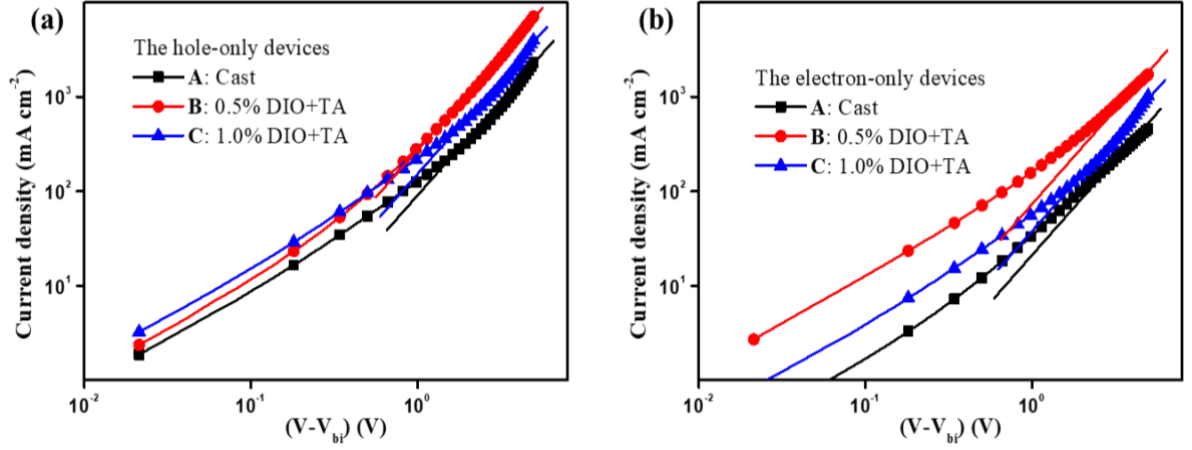


Figure 2. *J-V* characteristics of hole-only (a) and electron-only (b) devices under dark conditions. The bold lines with a slope of 2 mark the SCLC regions.

To further obtain detailed insight into recombination processes, the carrier density and lifetime were determined by charge extraction (CE).²⁷ and transient photovoltage (TPV)²⁸ methods under various V_{oc} conditions as adjusted by light bias, respectively. The function of V_{oc} versus illumination intensities (I) was also determined in Figure S4, the V_{oc} of three devices revealed similar variation trend under the varying illumination. The relationship between the extracted carrier density from CE and V_{oc} is presented in Figure 3a. According to

the function of $\tau_{\Delta n} = \tau_{\Delta n_0} e^{-\beta V_{oc}}$, $\tau_{\Delta n_0}$ is carrier lifetime without illumination and β is a constant, respectively.²⁹⁻³⁰ The fitted β values of devices A, B and C are 8.97, 11.54 and 9.89 V^{-1} , respectively. Device B exhibited the highest decay order. Moreover, the function of charge

density versus varying V_{oc} can be depicted by $n = n_0 e^{\gamma V_{oc}}$, where n_0 is the charge carrier density under dark and γ is a constant, respectively.³¹ The experimental results are presented in Figure 3b. From the deduced data, n_0 is $8.8 \times 10^{12} \text{ cm}^{-3}$ and γ is 4.40 V^{-1} for the device A, n_0 is $3.4 \times 10^{14} \text{ cm}^{-3}$ and γ is 3.57 V^{-1} for the device B, n_0 is $9.6 \times 10^{13} \text{ cm}^{-3}$ and γ is 3.88 V^{-1} for the device C, respectively. Based on the above device parameters, although the V_{oc} of device B and C are lower compared to device A, the charge density is obviously enhanced both in dark

and operation conditions generating the high J_{sc} . The extracted parameters are summarized in Table S3. Combining the determined carrier lifetime and carrier density, the function of them was shown in Figure 3c, the function of extracted lifetime vs charge density exhibited power law dependence. At the same carrier density condition, the lifetimes of devices were in the sequence $A > C > B$. In addition, the non-geminated recombination rate coefficient³²

$k_{rec}(n) = 1 / (1 + \frac{\beta}{\gamma}) n \tau_{\Delta n}$ could also be calculated, the Figure 3d showed the characteristic curves of carrier density versus k_{rec} . Although having the lowest carrier density, the k_{rec} of device A was highest among of them. The optimal device B possessed the lowest k_{rec} and highest carrier density. Even if at the same carrier density condition, the k_{rec} of devices were also in the sequence $A > C > B$ in Figure 3d. As described formerly, the improved mobility and weakened k_{rec} can enhance the carrier transport and restrain the non-geminate recombination, realizing the highest J_{sc} and FF in the device B with optimal DIO content.³³ Hence, there is a close correlation between the carrier dynamics and the content of DIO. To fabricated the high-performance device, the DIO concentration is carefully modulated.

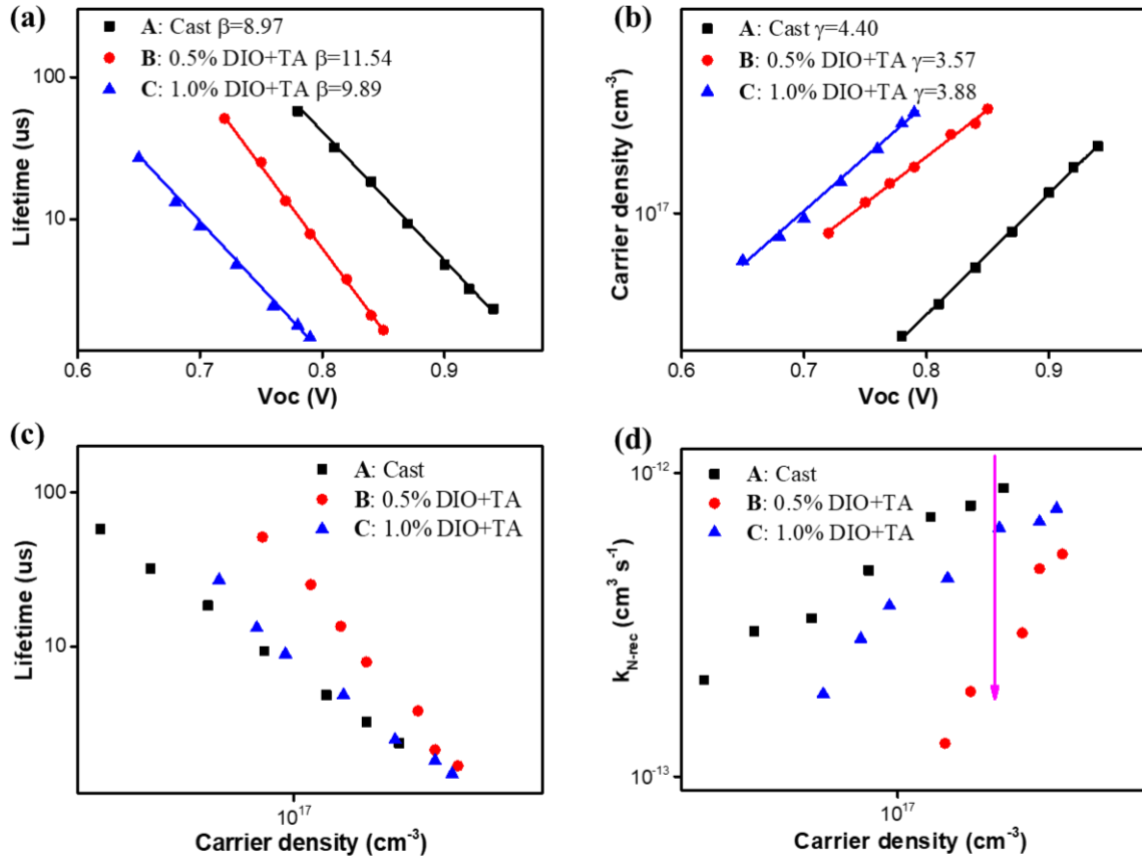


Figure 3. Extracted carrier lifetime (a) and carrier density (b) of devices under different V_{oc} conditions by adjusted light bias; the carrier lifetime (c) and k_{rec} (d) versus the carrier density for the investigated devices.

The generation and separation of excitons, charge transport and recombination are strongly linked with the morphology of BHJ film^{4, 22}. To explore the influence of the DIO content on the microstructure of PBDBT2F:IT4F blend films, we employed the grazing incidence wide-angle X-ray scattering (GIWAXS) technique to obtain information about the molecular packing and ordering.³⁴ Diffraction patterns and deduced line-cuts of the blend films are presented in Figure 4. For the as-cast film it was difficult to find an apparent π - π (010) stacking peak at required region and prohibited the mixed orientation of “edge-on” and “face-on”. In contrast, the film from device B showed apparent π - π (010) stacking peak at $q = 1.77 \text{ \AA}^{-1}$. The calculated π - π stacking distance is 3.55 \AA in the out-of-plane (OOP) direction, the prominent “face-on” in the mixed orientation was also observed from the diffraction pattern. The largely enhanced

proportion of “face-on” packing is considered to facilitate the charge transport in vertical direction in keeping with the build-in field direction, improving the effective transport and thus to reduce the probability of carrier recombination and other loss modes. Upon further increasing the DIO amount in the solvent, the film from device C also exhibited the π - π stacking peak at $q = 1.80 \text{ \AA}^{-1}$, the π - π stacking distance reduced to 3.48 \AA . The shortened stacking distance is also a factor to the reduction of V_{oc} in the device C. In addition, the “face-on” proportion in the mixed orientation was lowered compared to the film of device B. The non-uniform packing behavior is poor for the charge transport, generating the decrease of J_{sc} and FF in device C. On the other hand, the all the blend films had lamellar (100) diffraction peaks with $q = 0.30 \text{ \AA}^{-1}$ in the in-plane (IP) direction, but the peaks shapes were narrowed along with increase of DIO content. The full width at half-maximum (fwhm) of the diffraction peaks (fwhm-A = 0.054 \AA^{-1} , fwhm-B = 0.027 \AA^{-1} , and fwhm-C = 0.017 \AA^{-1} , respectively) imply that the crystallite sizes of blend films were in the sequence $A < B < C$.³⁴ The advisable enlarged size is helpful to promote charge transport, consistent with the determined carrier mobility of the devices. Combining the structural information with the device performance, we may speculate that higher DIO contents induce the stronger aggregation and extended domains in the blend films, which could produce the tortuosity in the molecule packing. To support to this conjecture, atomic force microscopy (AFM) in tapping mode was performed to investigate the surface morphology of these films. From the Figure S5, the degree of aggregation was enhanced upon increase of DIO content. Especially film C showed intense aggregation and higher root-mean-square roughness (RMS) with a value of 3.19 nm . The coarser film hinders the charge transport and collection in the device in agreement with the above device performances.³⁵ Thus, the addition of DIO to the solvent is a feasible approach to optimize the film morphology, however, the content needs to be controlled accurately.

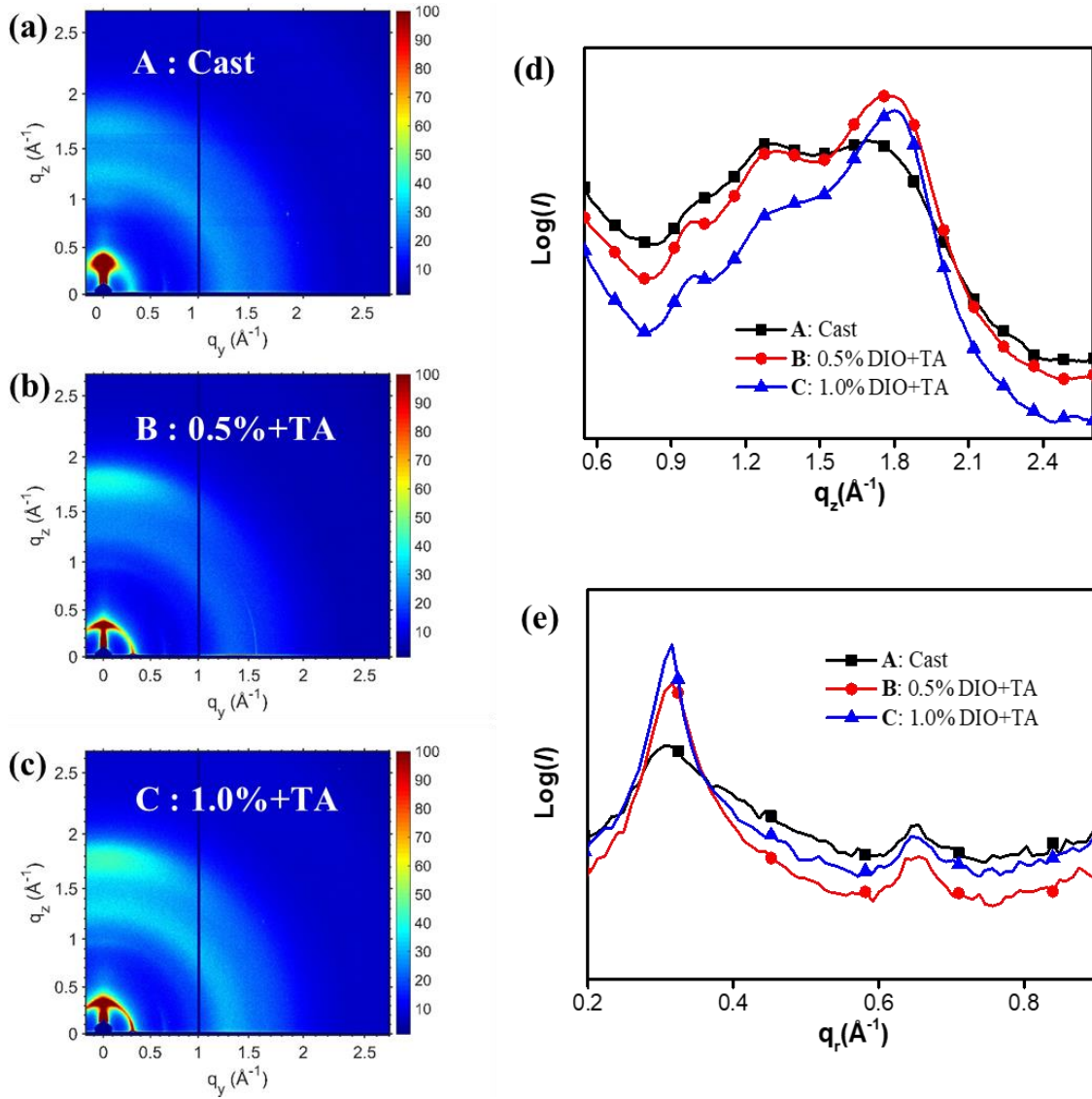


Figure 4. GIWAXS patterns of PBDBT2Cl:T4F films with various DIO content processing (a,b c); the corresponding line-cuts in the out-of-plane (d) and in-plane (e) directions.

In this work, the impact of DIO on carrier dynamics and morphology in PBDBT2Cl:IT4F system were investigated comprehensively. The V_{oc} of devices were monotonous declined by gradually increasing DIO content, while J_{sc} and FF showed maximum values at 0.5% DIO content. The champion devices were obtained by using 0.5% DIO resulting in a PCE of 13.14%. Through steady and transient dynamics tests, we could show that aDIO content of 0.5% improves the hole and electron mobility. Thus, the quasi-Fermi levels between electrons and holes shorten, while the non-geminate recombination of carriers was also restrained at high carrier density condition. In addition, the film with 0.5% DIO processing showed favorable

“face-on” orientation as derived from GIWAXS patterns. The advisable enlarged crystallite-sizes was also formed by desired DIO content. However, excess DIO content produced intense aggregation and dilated size of domains in the blend films causing tortuosity in the molecule packing thus reducing carrier transport and intensive recombination of carriers in devices. This study evidences that the required DIO content can produce positive effects on performance of device, giving a fundamental guideline into the use of DIO additives on carrier dynamics and morphology of non-fullerene PSCs.

Acknowledgments

^{||}H. C. And J. Q. contributed equally to this work. The authors acknowledge financial support from SUSTech, the Recruitment Program of Global Youth Experts of China, the National Natural Science Foundation of China (51773087, 21733005), the Natural Science Foundation of Guangdong Province (2016A030313637), Shenzhen Fundamental Research program (JCYJ20170817111214740) and Shenzhen Nobel Prize Scientists Laboratory Project (C17213101). W. C. gratefully acknowledges financial support from the US Department of Energy, Office of Science, Materials Science and Engineering Division. We also thank Drs. Joseph Strzalka and Zhang Jiang for the assistance with GIWAXS measurements. Use of the Advanced Photon Source (APS) at the Argonne National Laboratory was supported by the U.S. Department of Energy, Office of Science, Office of Basic Energy Sciences, under contract no. DE-AC02-06CH11357.

Supporting Information

The Supporting Information is available free of charge on the ACS Publications website. It includes experimental details, device characterization, tables of related device data, and AFM images (PDF).

References

- (1) Hou, J.; Inganäs, O.; Friend, R. H.; Gao, F. Organic Solar Cells Based on Non-fullerene Acceptors. *Nat. Mater.* **2018**, *17*, 119
- (2) He, Z.; Xiao, B.; Liu, F.; Wu, H.; Yang, Y.; Xiao, S.; Wang, C.; Russell, T. P.; Cao, Y. Single-junction Polymer Solar Cells with High Efficiency and Photovoltage. *Nat. Photon.* **2015**, *9*, 174-179.
- (3) Li, Y. Molecular Design of Photovoltaic Materials for Polymer Solar Cells: Toward Suitable Electronic Energy Levels and Broad Absorption. *Acc. Chem. Res.* **2012**, *45*, 723-733.
- (4) Liu, Y.; Zhao, J.; Li, Z.; Mu, C.; Ma, W.; Hu, H.; Jiang, K.; Lin, H.; Ade, H.; Yan, H. Aggregation and Morphology Control Enables Multiple Cases of High-efficiency Polymer Solar Cells. *Nat. Commun.* **2014**, *5*, 5293.
- (5) Kan, B.; Li, M.; Zhang, Q.; Liu, F.; Wan, X.; Wang, Y.; Ni, W.; Long, G.; Yang, X.; Feng, H.; et al. A Series of Simple Oligomer-like Small Molecules based on Oligothiophenes for Solution-processed Solar Cells with High Efficiency. *J. Am. Chem. Soc.* **2015**, *137*, 3886-3893.
- (6) Lin, Y.; Zhan, X. Oligomer Molecules for Efficient Organic Photovoltaics. *Acc. Chem. Res.* **2016**, *49*, 175-183.
- (7) Liu, J.; Chen, S.; Qian, D.; Gautam, B.; Yang, G.; Zhao, J.; Bergqvist, J.; Zhang, F.; Ma, W.; Ade, H.; et al. Fast Charge Separation in a Non-fullerene Organic Solar Cell with a Small Driving Force. *Nat. Energy* **2016**, *1*, 16089.
- (8) Guo, X.; Zhou, N.; Lou, S. J.; Smith, J.; Tice, D. B.; Hennek, J. W.; Ortiz, R. P.; Navarrete, J. T. L.; Li, S.; Strzalka, J.; et al. Polymer Solar Cells with Enhanced Fill Factors. *Nat. Photon.* **2013**, *7*, 825-833.
- (9) Zhao, J.; Li, Y.; Yang, G.; Jiang, K.; Lin, H.; Ade, H.; Ma, W.; Yan, H. Efficient organic solar cells processed from hydrocarbon solvents. *Nat. Energy* **2016**, *1*, 15027.

- (10) Li, H.; Xiao, Z.; Ding, L.; Wang, J. Thermostable Single-junction Organic Solar Cells with a Power Conversion Efficiency of 14.62%. *Sci. Bull.* **2018**, *63*, 340-342.
- (11) Zhang, H.; Yao, H.; Hou, J.; Zhu, J.; Zhang, J.; Li, W.; Yu, R.; Gao, B.; Zhang, S.; Hou, J. Over 14% Efficiency in Organic Solar Cells Enabled by Chlorinated Nonfullerene Small-Molecule Acceptors. *Adv. Mater.* **2018**, *30*, 1800613.
- (12) Xiao, Z.; Jia, X.; Ding, L. Ternary Organic Solar Cells offer 14% Power Conversion Efficiency. *Sci. Bull.* **2017**, *62*: 1562-1564.
- (13) Li, S.; Ye, L.; Zhao, W.; Yan, H.; Yang, B.; Liu, D.; Li, W.; Ade, H.; Hou, J. A Wide Band Gap Polymer with a Deep Highest Occupied Molecular Orbital Level Enables 14.2% Efficiency in Polymer Solar Cells. *J. Am. Chem. Soc.* **2018**, *140*, 7159-7167.
- (14) Che, X.; Li, Y.; Qu, Y.; Forrest, S. R. High Fabrication Yield Organic Tandem Photovoltaics Combining Vacuum- and Solution-processed Subcells with 15% Efficiency. *Nat. Energy* **2018**, *3*, 422-427.
- (15) Zhang, S.; Qin, Y.; Zhu, J.; Hou, J. Over 14% Efficiency in Polymer Solar Cells Enabled by a Chlorinated Polymer Donor. *Adv. Mater.* **2018**, *30*, 1800868. (16) Chen, H.; Hu, Z.; Wang, H.; Liu, L.; Chao, P.; Qu, J.; Liu, A.; Chen, W.; He, F. A Chlorinated π -Conjugated Polymer Donor for Efficient Organic Solar Cells. *Joule* **2018**, *2*, 1623-1634.
- (17) Mo, D.; Wang, H.; Chen, H.; Qu, S.; Chao, P.; Yang, Z.; Tian, L.; Su, Y.-A.; Gao, Y.; Yang, B.; et al. Chlorination of Low-Band-Gap Polymers: Toward High-Performance Polymer Solar Cells. *Chem. Mater.* **2017**, *29*, 2819-2830.
- (18) Chao, P.; Mu, Z.; Wang, H.; Mo, D.; Chen, H.; Meng, H.; Chen, W.; He, F. Chlorination of Side Chains: A Strategy for Achieving a High Open Circuit Voltage Over 1.0 V in Benzo[1,2-b:4,5-b']dithiophene-Based Non-Fullerene Solar Cells. *ACS Appl. Energy Mater.* **2018**, *1*, 2365-2372.

- (19) Lou, S. J.; Szarko, J. M.; Xu, T.; Yu, L.; Marks, T. J.; Chen, L. X. Effects of Additives on the Morphology of Solution Phase Aggregates Formed by Active Layer Components of High-Efficiency Organic Solar Cells. *J. Am. Chem. Soc.* **2011**, *51*, 20661–20663.
- (20) Li, G.; Shrotriya, V.; Huang, J.; Mariarty, T.; Emery, K.; Yang, Y. High-Efficiency Solution Processable Polymer Photovoltaic Cells by Self-Organization of Polymer Blends. *Nat. Mater.* **2005**, *4*, 864–868.
- (21) Xu, S.; Feng, L.; Yuan, J.; Zhang, Z.-G.; Li, Y.; Peng, H.; Zou, Y. Hexafluoroquinoxaline Based Polymer for Nonfullerene Solar Cells Reaching 9.4% Efficiency. *ACS Appl. Mater. Interfaces* **2017**, *9*, 18816–18825.
- (22) Du, X. Y.; Jiao, X.; Rechberger, S.; Perea, J. D.; Meyer, M.; Kazerouni, N.; Spiecker, E.; Ade, H.; Brabec, C. J.; Fink, R. H.; **et al.** Crystallization of Sensitizers Controls Morphology and Performance in Si-/C-PCPDTBT-Sensitized P3HT:ICBA Ternary Blends. *Macromolecules* **2017**, *50*, 2415-2423.
- (23) Zhao, W. C.; Li, S. S.; Yao, H. F.; Zhang, S. Q.; Zhang, Y.; Yang, B.; Hou, J. H. Molecular Optimization Enables over 13% Efficiency in Organic Solar Cells. *J. Am. Chem. Soc.* **2017**, *139*, 7148–7151.
- (24) Murgatroyd, P. N. Theory of Space-Charge-Limited Current Enhanced by Frenkel Effect. *J. Phys. D: Appl. Phys.* **1970**, *3*, 151-156.
- (25) Chen, H.; Miao, J.; Yan, J.; He, Z.; Wu, H. Improving Organic Solar Cells Efficiency Through a Two-Step Method Consisting of Solvent Vapor Annealing and Thermal Annealing. *IEEE J. Sel. Top. Quantum Electron.* **2016**, *22*, 66–72.
- (26) Kyaw, A. K. K.; Wang, D. H.; Luo, C.; Cao, Y.; Nguyen, T.-Q.; Bazan, G. C.; Heeger, A. J. Effects of Solvent Additives on Morphology, Charge Generation, Transport, and Recombination in Solution-Processed Small-Molecule Solar Cells. *Adv. Energy Mater.* **2014**, *4*, 1301469.
- (27) Shuttle, C. G.; O'Regan, B.; Ballantyne, A. M.; Nelson, J.; Bradley, D. D. C.; de Mello, J.; Durrant, J. R. Experimental Determination of the Rate Law for Charge Carrier Decay in a

Polythiophene: Fullerene Solar cell. *Appl. Phys. Lett.* **2008**, *92*, 093311.

(28) Maurano, A.; Hamilton, R.; Shuttle, C. G.; Ballantyne, A. M.; Nelson, J.; O'Regan, B.; Zhang, W.; McCulloch, I.; Azimi, H.; Morana, M.; et al. Recombination Dynamics as a Key Determinant of Open Circuit Voltage in Organic Bulk Heterojunction Solar Cells: a Comparison of Four Different Donor Polymers. *Adv. Mater.* **2010**, *22*, 4987–4992.

(29) Xie, Y.; Yu, Y.; Liang, Q.; Wan, J-H.; Wu, H.; Cao, Y. Understanding the Enhanced Open-Circuit Voltage of Polymer Solar Cells Based on a Diketopyrrolopyrrole Small Molecular Acceptor. *ACS Appl. Mater. Interfaces* **2018**, *10*, 25589–25593

(30) Kirchartz, T.; Nelson, J. Meaning of Reaction Orders in Polymer:fullerene Solar Cells. *Phys. Rev. B: Condens. Matter Mater. Phys.* **2012**, *86*, 165201.

(31) Ryan, J. W.; Marin-Beloqui, J. M.; Albero, J.; Palomares, E. Nongeminate Recombination Dynamics-Device Voltage Relationship in Hybrid PbS Quantum Dot/C₆₀ Solar Cells. *J. Phys. Chem. C* **2013**, *117*, 17470–17476.

(32) Credginton, D.; Hamilton, R.; Atienzar, P.; Nelson, J.; Durrant, J. R. Non-Geminate Recombination as the Primary Determinant of Open-Circuit Voltage in Polythiophene:Fullerene Blend Solar Cells: an Analysis of the Influence of Device Processing Conditions. *Adv. Funct. Mater.* **2011**, *21*, 2744–2753.

(33) Wheeler, S.; Bryant, D.; Troughton, J.; Kirchartz, T.; Watson, T.; Nelson, J.; Durrant, J. R. Transient Optoelectronic Analysis of the Impact of Material Energetics and Recombination Kinetics on the Open-Circuit Voltage of Hybrid Perovskite Solar Cells. *J. Phys. Chem. C* **2017**, *121*, 13496–13506.

(34) Hu, Z.; Chen, H.; Qu, J.; Zhong, X.; Chao, P.; Xie, M.; Lu, W.; Liu, A.; Tian, L.; Su, Y.-A.; et al. Design and Synthesis of Chlorinated Benzothiadiazole-Based Polymers for Efficient Solar Energy Conversion. *ACS Energy Lett.* **2017**, *2*, 753-758.

(35) Wang, J.; Liu, K.; Yan, J.; Wu, Z.; Liu, F.; Xiao, F.; Chang, Z.; Wu, H.; Cao, Y.; Russell, T. P. Series of Multifluorine Substituted Oligomers for Organic Solar Cells with Efficiency

over 9% and Fill Factor of 0.77 by Combination Thermal and Solvent Vapor Annealing. *J. Am. Chem. Soc.* **2016**, *138*, 7687–7697.